Ultrashort-pulse propagation through free-carrier plasmas

Jeremy R. Gulley and W. M. Dennis*
Department of Physics and Astronomy, University of Georgia, Athens, Georgia 30602
(Received 4 August 2009; published 10 March 2010)

The past decade has seen frequent use of a modified nonlinear Schrödinger equation to describe ultrashort pulse propagation in materials where free-carrier plasmas are present. The optical contribution from the resulting free-current densities in this equation is often described using a classical Drude model. However, the ultimate form of this contribution in the modified nonlinear Schrödinger equation is somewhat inconsistent in the literature. We clarify this ambiguity by deriving the modified nonlinear Schrödinger equation from the classical wave equation containing a free-current density contribution. The Drude model is then used to obtain an expression for the complex free-carrier current density envelope with temporal dispersion corrections for ultrashort laser pulses. These temporal dispersion corrections to the current-density term differ, to our knowledge, from all other models in the literature in that they depend more sensitively on the value of the Drude free-carrier collision time. These corrections reduce to the current models in the literature for limiting cases. Theoretical analysis and computer simulations show that these differences can significantly affect the dynamic interactions of plasma absorption and plasma defocusing for materials with free-carrier collision times on the order of one optical cycle (or less) of the applied field.

DOI: 10.1103/PhysRevA.81.033818 PACS number(s): 42.65.Sf, 42.65.Re, 52.38.Hb

I. INTRODUCTION

In the past decade there has been significant interest in the precise modification of materials on both the micrometer and nanometer length scales [1–6]. High-intensity, ultrashort laser pulses are now used in micromachining and nanostructuring applications, because of the ability to make precise material modifications both on the surface and in the bulk, often while avoiding the onset of irreversible structural damage to the material [7]. Ultrashort laser pulses are also an important tool for discovering fundamental information about optical and material processes that occur on time scales approaching the limit of one optical cycle of the applied laser field [8,9]. The widespread use of ultrashort pulses for these purposes necessitates the development of a more detailed and fundamental description of free-carrier effects in the femtosecond time regime [10,11]. Ultimately, this must involve a systematic investigation of the interplay between high-intensity ultrashort pulse propagation and the presence of free-carrier plasmas within the material [12,13]. For linearly polarized laser pulses, a scalar electric field envelope equation has proven to be an accurate and efficient method of describing ultrashort pulse propagation in a variety of isotropic nonlinear materials [9,14].

Nonlinear envelope equations have been used to model high-intensity laser pulse propagation for over three decades [15–18]. A basic nonlinear Schrödinger equation (NLSE) can account for optical diffraction, dispersion, and a Kerr-type nonlinear polarization [19]. As laser pulses became progressively shorter in duration and correspondingly stronger in intensity, authors found it necessary to account for high-order energetic and temporal effects [14]. The energetic (high-intensity) corrections include high-order nonlinearities, multiphoton absorption, and free-carrier effects [14]. Temporal corrections to the NLSE can be largely attributed to two articles. In the first of these articles, Blow and Wood [20] provide a basic model for temporal delay of the nonlinear response, for the material of fused silica in particular. In the second of these articles, Brabec and Krausz [9] derive a nonlinear envelope equation valid for laser pulses as short as one optical cycle in duration. This modified NLSE accounts for high-order dispersion, linear shock, and self-steepening without actually specifying the form of the nonlinear polarization, allowing for a direct incorporation of the Blow and Wood model for nonlinear delay.

The inclusion of nonlinear delay and high-order energetic corrections to the nonlinear polarization in the modified NLSE of Ref. [9] is straightforward. However, inclusion of free-carrier effects is somewhat ambiguous, as a free-current density term was not included in the original wave equation from which the modified NLSE was derived [9]. Contributions of a Drude free-carrier current density to the modified NLSE to date have frequently been of the form [5,7,21,22],

$$\left[\frac{\partial \xi}{\partial z}\right]_{fc} = -\frac{\sigma}{2}(1+i\omega_0\tau_c)\hat{T}^{-1}[\rho\xi] \ , \tag{1}$$

where ξ is the complex electric field envelope, z is the propagation axis, $\sigma = q^2\tau_c/n_0 c\epsilon_0 m(1+\omega_0^2\tau_c^2)$ is the cross section of inverse Bremsstrahlung absorption, $n_0 = k_0 c/\omega_0$ is the linear index of refraction, q is the free-carrier charge, c is the speed of light in a vacuum, τ_c is the free-carrier collision time, ω_0 is the carrier frequency of the field, ρ is the time-dependent free-carrier density, and $\hat{T}^{-1}$ is the inverse of a steepening operator $\hat{T} = 1 + (i/\omega_0)\partial_t$ as defined in Ref. [9]. The inverse steepening operator in Eq. (1) is sometimes assumed to be unity for longer pulses (i.e., $\hat{T}^{-1} \to 1$), a zeroth temporal order approximation common in the literature [23–25]. In other recent articles the inverse steepening operator is attached only to the imaginary part of Eq. (1) [26,27]. We have investigated this matter and have found that Eq. (1), and all the other aforementioned free-carrier contributions, are limiting cases of a more general Drude

*bill@physast.uga.edu

free-carrier contribution:

$$\left[\frac{\partial \xi}{\partial z}\right]_{fc} = -\frac{\sigma}{2}(1+i\omega_0\tau_c)\hat{G}^{-1}[\rho\xi] \ , \tag{2}$$

where $\hat{G}^{-1}$ is the inverse of a free-carrier dispersion operator $\hat{G} = 1 + (i/\omega_0)g\partial_t$ derived in this article. Here, $g = -i\omega_0\tau_c/(1 - i\omega_0\tau_c)$ is a dimensionless complex constant that distinguishes the free-carrier operator $\hat{G}$ from the steepening operator $\hat{T}$. The time derivative coefficient of the $\hat{T}$ operator depends only on the carrier frequency ω_0, whereas the $\hat{G}$ operator additionally depends on the electron collision time τ_c, which is a material parameter from the Drude model. We also demonstrate that Eq. (1) is an accurate approximation of Eq. (2) only in the limiting case where the collision time is much greater than an optical cycle of the applied field. Under such conditions these results suggest that the full Drude model corrections of Eq. (2) are required to accurately describe the propagation of ultrashort laser pulses through free-carrier plasmas. This not only includes the pulses whose temporal widths approach one optical cycle, but also any ultrashort pulse whose initial temporal shape is steepened by linear or nonlinear shock, as well as laser-plasma interactions that occur during the process of filamentation [7,27,28].

In this article we present the derivation of a modified NLSE with a Drude free-current density contribution following the method of Ref. [9]. The resulting equation shows that the contribution of free carriers is given by Eq. (2), results of which are in turn compared analytically with the results predicted by Eq. (1). Results from simulations that solve the modified NLSE in fused silica below the threshold of permanent optical damage are also presented and Eqs. (1) and (2) are compared as descriptions of free-carrier effects.

II. DERIVATION OF A MODIFIED NLSE WITH A FREE-CURRENT DENSITY

A linearly polarized laser pulse propagating through a nonlinear isotropic medium with free carriers can be described by the following wave equation [9,27]:

$$\nabla^2\vec{E} - \frac{1}{c^2}\frac{\partial^2\vec{E}}{\partial t^2} = \mu_0\frac{\partial^2\vec{P}}{\partial t^2} + \mu_0\frac{\partial\vec{J}_F}{\partial t}. \tag{3}$$

Here c is the speed of light in a vacuum and $\vec{E}$ is the electric field that satisfies the condition $\vec{\nabla}\cdot\vec{E} = 0$ [27]. On the right-hand side of Eq. (3) are the two source terms where $\vec{P}$ is the total polarization and represents the optical contribution of bound charges, while $\vec{J}_F$ is the free-current density and represents the optical contribution of free carriers. The nonlinear polarization, $\vec{P}_{NL}$, is considered to be a perturbation to the linear polarization, $\vec{P}_L$, such that $\vec{P} = \vec{P}_L + \vec{P}_{NL}$.

A. The nonlinear envelope equation

Equation (3) is expressed in terms of a linear displacement field $\vec{D}_L = \epsilon_0\vec{E} + \vec{P}_L$. The resulting expression is Fourier transformed into the frequency domain where $\tilde{\vec{D}}_L(\omega) = \epsilon_0(c^2/\omega^2)\tilde{\kappa}^2(\omega)\tilde{\vec{E}}(\omega)$ and $\tilde{\kappa}(\omega) = \tilde{k}(\omega) + i\tilde{\alpha}(\omega)/2$ is the complex linear wave vector, $\tilde{k}$ is the real part of the wave vector, and $\tilde{\alpha}$ is the intensity-based absorption coefficient.

$$\nabla^2\tilde{\vec{E}} + \tilde{\kappa}^2\tilde{\vec{E}} = -\mu_0\omega^2\tilde{\vec{P}}_{NL} - i\omega\mu_0\tilde{\vec{J}}_F. \tag{4}$$

Next, all vectors are expressed in complex notation and in terms of their respective complex envelope functions:

$$\vec{E}(\vec{x},t) = \tfrac{1}{2}[\xi(\vec{x},t)\,e^{i(k_0z-\omega_0t)} + \text{c.c.}]\hat{x}, \tag{5a}$$

$$\vec{P}_{NL}(\vec{x},t) = \tfrac{1}{2}[p_{nl}(\vec{x},t)\,e^{i(k_0z-\omega_0t)} + \text{c.c.}]\hat{x}, \tag{5b}$$

$$\vec{J}_F(\vec{x},t) = \tfrac{1}{2}[j_f(\vec{x},t)\,e^{i(k_0z-\omega_0t)} + \text{c.c.}]\hat{x}, \tag{5c}$$

where ω_0 is the carrier frequency, k_0 is the real part of the complex wave vector, that is, $\text{Re}[\tilde{\kappa}(\omega_0)]$, and z is the propagation axis. Equations (5a)–(5c) are Fourier transformed to the frequency domain and substituted into Eq. (4). The derivatives along the propagation axis are then taken, the backward propagating elements are neglected, and the scalar product with the $\hat{x}$ direction is taken to yield a scalar expression in terms of the envelope functions.

$$\begin{aligned}&\left[\nabla_\perp^2 + \partial_z^2 + 2ik_0\partial_z + \tilde{\kappa}^2(\omega) - k_0^2\right]\tilde{\xi}(\vec{x},\omega-\omega_0)\\ &\quad = -\omega^2\mu_0\tilde{p}_{nl}(\vec{x},\omega-\omega_0) - i\omega\mu_0\tilde{j}_f(\vec{x},\omega-\omega_0).\end{aligned} \tag{6}$$

$\tilde{\kappa}(\omega)$ is Taylor expanded about the carrier frequency ω_0, and Eq. (6) is inverse Fourier transformed back into the time domain. The equation is then further transformed into the retarded time frame traveling at the group velocity $v_g = 1/\partial_\omega\tilde{k}(\omega_0)$ of the pulse; that is, $z' = z$ is the transformed propagation axis and $\tau = t - z/v_g$ is the retarded time coordinate. The equation is now rearranged to read

$$\begin{aligned}&\left(\nabla_\perp^2 + \partial_{z'}^2 + 2ik_0\hat{U}\partial_{z'} + 2k_0\hat{U}\hat{D}_b + \hat{D}_b^2\right)\xi(\vec{x},\tau)\\ &\quad = -\mu_0\omega_0^2\hat{T}^2p_{nl}(\vec{x},\tau) - i\mu_0\omega_0\hat{T}j_f(\vec{x},\tau),\end{aligned} \tag{7}$$

where $\hat{D}_b$ is the bound charge linear dispersion operator, and $\hat{U}$ and $\hat{T}$ are steepening operators defined by

$$\hat{D}_b = i\frac{\alpha_0}{2} - \frac{\alpha_1}{2}\partial_\tau + \sum_{m=2}^{\infty}\frac{k_m + i\alpha_m/2}{m!}(i\partial_\tau)^m \tag{8a}$$

$$\hat{U} = 1 + i\frac{k_1}{k_0}\partial_\tau \tag{8b}$$

$$\hat{T} = 1 + i\frac{1}{\omega_0}\partial_\tau, \tag{8c}$$

where $k_m = \partial^m\tilde{k}/\partial\omega^m|_{\omega_0}$ and $\alpha_m = \partial^m\tilde{\alpha}/\partial\omega^m|_{\omega_0}$. The slowly varying-wave approximation (SVWA) is now applied, that is, $|\partial_{z'}E| \ll k_0|E|$, allowing us to neglect the second-order derivative along the propagation axis [9]. The equation is then rearranged to read

$$\begin{aligned}\hat{U}\frac{\partial\xi}{\partial z'} = i&\left[\frac{\nabla_\perp^2}{2k_0} + \left(\hat{U} + \frac{\hat{D}_b}{2k_0}\right)\hat{D}_b\right]\xi(\vec{x},\tau)\\ &+ i\frac{\omega_0}{2n_0\epsilon_0c}\hat{T}^2p_{nl}(\vec{x},\tau) - \frac{\hat{T}}{2n_0\epsilon_0c}j_f(\vec{x},\tau).\end{aligned} \tag{9}$$

In principle, this equation may now be solved for the pulse envelope ξ once p_{nl} and j_f are specified. Equation (9) is in fact the nonlinear envelope equation used by some authors in the literature [7,21,29–31]. However, it is common to make additional approximations that simplify this expression. In transparent materials, it is generally the case

that $(\hat{D}_b/2k_0)\xi \ll \xi$. Furthermore, the SVWA requires that the condition $|1-\omega_0 k_1/k_0| \ll 1$ be satisfied in order to describe propagation of pulses with temporal durations approaching the limit of one optical cycle [9]. If this criterion is satisfied, then the approximation $\hat{U} \approx \hat{T}$ becomes applicable. In fused silica, for example, $\omega_0 k_1/k_0 \approx 1.0095$ for 800-nm light and the above condition is sufficiently satisfied. Once these approximations are applied, the equation is multiplied by the inverse steepening operator $\hat{T}^{-1}$ and takes the simpler form:

$$\frac{\partial \xi}{\partial z'} = \left(\frac{i}{2k_0}\hat{T}^{-1}\nabla_\perp^2 + i\hat{D}_b\right)\xi(\vec{x},\tau) + i\frac{\omega_0\,\hat{T}}{2n_0\epsilon_0 c}p_{nl}(\vec{x},\tau) - \frac{j_f(\vec{x},\tau)}{2n_0\epsilon_0 c}. \tag{10}$$

Equation (10) is now identical to the nonlinear envelope equation derived in Ref. [9], but in System International (SI) units and with the addition of a free-current density term. It is notable that no steepening operators act on the free-current density envelope.

This does not mean to imply that there are no temporal corrections necessary to correctly account for ultrashort pulses propagating through a free-carrier plasma, as per the zeroth-order approximation of Eq. (1). However, if such corrections are necessary, Eq. (10) predicts that they must arise from within the free-current density envelope itself. Such corrections will depend explicitly on the model one uses to calculate the free-current density. Also, if multiple sources of free-current densities exist (e.g., a free-electron gas or an ionization current) then j_f represents the sum of all of their individual contributions. As specific examples, envelopes for a Drude-type free-current density as well as a photoionization current will be derived in the following subsections.

B. The photoionization current density envelope

An important process in high-intensity laser pulse propagation is photoionization, which often produces the first free charges in an otherwise neutral, nonconducting material [13]. In a strongly insulating medium this may require the simultaneous absorption of multiple photons to excite an electron from the valence band to the conduction band. If the instantaneous intensity within the pulse is in excess of $\sim 10^{14}\,\mathrm{W/cm^2}$, then ionization processes can become strongly dependent on the absolute phase of the pulse, thereby invalidating an envelope treatment in this regime [8]. However, at lower intensities a time-averaged photoionization absorption is ubiquitous in the modified NLSEs of the literature. Here, there also exists some ambiguity in the form of this contribution (see, e.g., Refs. [5,21,23,32]). We therefore derive an expression for the complex envelope of a time-averaged photoionization current density $\vec{J}_{\mathrm{PI}}(\vec{x},t)$.

The optical power loss per volume from photoionization is $\vec{J}_{\mathrm{PI}}\cdot\vec{E}$. This quantity, when time-averaged, is expressed in complex envelope notation and directly related to the energy required for valence electrons to cross the forbidden gap U at a number per volume photoionization rate of W_{PI}; $(1/2)j_{\mathrm{pi}}^*\,\xi = W_{\mathrm{PI}}U$ [33], where j_{pi} is the photoionization current density envelope. In terms of the intensity $I=(1/2)n_0\epsilon_0 c|\xi|^2$, the resulting current density envelope in the retarded time frame is

$$j_{\mathrm{pi}}(\vec{x},\tau) = n_0\epsilon_0 c\,\frac{W_{\mathrm{PI}}U}{I}\xi(\vec{x},\tau). \tag{11}$$

Equation (11), when substituted into Eq. (9) or Eq. (10), is in agreement with the form of the photoionization contribution to the modified NLSE most commonly used in the literature [7,21,22,24–27,29–31,34].

C. The Drude free-current density envelope

An expression for a plasma fluid contribution to the free-current density envelope $j_f(\vec{x},t)$ will now be derived. A current density vector for a free-carrier fluid $\vec{J}_{FC}$ in an electrically neutral medium can be described by an equation of force density according to the Drude model [27],

$$\frac{\partial}{\partial t}\vec{J}_{FC}(\vec{x},t) + \frac{1}{\tau_c}\vec{J}_{FC}(\vec{x},t) = \frac{q}{m}\vec{F}(\vec{x},t). \tag{12}$$

Here, τ_c is the characteristic free-carrier collision time, m and q are the respective mass and charge of the individual free carriers, $\vec{F}(\vec{x},t) = q\rho(\vec{x},t)\vec{E}(\vec{x},t)$ is the applied force density, and ρ is the free-carrier number density. Also, it is convenient to define $\vec{F}$ in complex envelope notation where $f(\vec{x},t) = q\rho(\vec{x},t)\xi(\vec{x},t)$ is the applied force density envelope function. Equation (12) is Fourier transformed into the frequency domain, the complex envelope expressions are substituted and phase matched, the scalar product with the $\hat{x}$ direction is taken, and the free-carrier current density envelope j_{fc} is related to the force density in frequency space.

$$\tilde{j}_{fc}(\vec{x},\omega-\omega_0) = \frac{q}{m}\left(\tau_c^{-1} - i\omega\right)^{-1}\tilde{f}(\vec{x},\omega-\omega_0). \tag{13}$$

The $(\tau_c^{-1}-i\omega)^{-1}$ quantity in Eq. (13) is Taylor expanded about ω_0 and the entire equation is inverse Fourier transformed back into the time domain. An investigation of the analyticity of the expansion in frequency space shows that it will converge for pulses as short as one optical cycle in duration as well as for all values of τ_c, making the result applicable in any situation where Eq. (10) is valid. After a transformation into the retarded time frame the final result is

$$j_{fc}(\vec{x},\tau) = \frac{q^2\tau_c}{m}\left(\frac{1+i\omega_0\tau_c}{1+\omega_0^2\tau_c^2}\right)\hat{G}^{-1}[\rho(\vec{x},\tau)\xi(\vec{x},\tau)], \tag{14}$$

where

$$\hat{G}^{-1} = \sum_{m=0}^{\infty}\left(\frac{-i}{\omega_0}g\partial_\tau\right)^m = \left(1+\frac{i}{\omega_0}g\partial_\tau\right)^{-1} \tag{15}$$

is the inverse free-charge dispersion operator in Eq. (2), and $g=(-i\omega_0\tau_c)/(1-i\omega_0\tau_c)$ is a dimensionless complex constant that distinguishes the operators $\hat{T}$ and $\hat{G}$. Substituting Eq. (14) into Eq. (10) gives the stated result of Eq. (2), where the cross section of inverse Bremsstrahlung absorption $\sigma = q^2\tau_c/n_0 c\epsilon_0 m(1+\omega_0^2\tau_c^2)$ and $n_0 = k_0 c/\omega_0$ is the linear index of refraction.

The dispersion corrections for free carriers as predicted by $\hat{G}$ are clearly distinct from the other steepening operators $\hat{T}$ and $\hat{U}$, in that the time derivative coefficient of $\hat{G}$ contains both real and imaginary parts. This distinguishing trait is

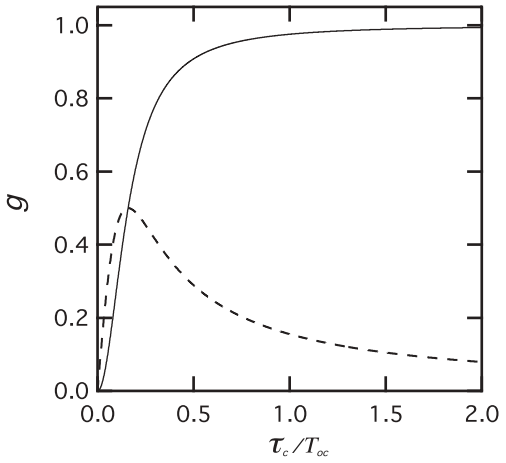

FIG. 1. The magnitude of the real (solid line) and the imaginary (dashed line) parts of the dimensionless constant g as a function of the characteristic free-carrier collision time τ_c scaled by the optical cycle T_{oc} of the applied field.

TABLE I. A list of electronic collision times τ_c provided in recent literature for experiments and simulations using 800-nm light. Collision times are shown in units of fs as well as number of optical cycles for the 800-nm wavelength. Also shown is the specific material for each collision time and references from which the collision times are taken or calculated.

τ_c (fs)	τ_c/T_{oc}	Materials	References
0.2	0.075	Fused silica	[35]
0.4	0.15	Fused silica, epithelium	[36]
0.7	0.26	Stroma	[36]
1.0	0.37	Fused silica	[25]
1.27	0.48	Fused silica	[5]
1.7	0.64	Fused silica	[37]
2.12	0.79	Sapphire	[32]
3.0	1.12	Water	[21]
10	3.8	Fused silica	[7,22]
20	7.5	Fused silica	[27]
23.3	9.4	Fused silica	[24]
350	112	Air	[23]

ultimately traceable to the different physical origins of the respective operators. The operator $\hat{T}$ originates from residual time derivatives on the right-hand side of Eq. (3), the operator $\hat{U}$ originates from linear dispersion relations of bound charges and a coordinate transformation, while $\hat{G}$ originates from dispersion relations of free charges according to the Drude model.

Since it has already been established that the approximation $\hat{U} \approx \hat{T}$ is widely applicable then perhaps the same is true of $\hat{G}$. This, however, would require that the constant $g \approx 1$, which is clearly not the case for collision times on the order of the optical cycle, $T_{oc} = 2\pi/\omega_0$, or less. Figure 1 shows the magnitude of the real and imaginary parts of g as a function of τ_c/T_{oc}. It is therefore worth examining whether collision times on the order of one optical cycle have been published in the recent literature. Table I shows a list of free-carrier collision times measured in experiment or used in simulation for a variety of materials in the recent literature. Note that many of these collision times are indeed on the order of one optical cycle or less.

It should be emphasized, however, that if one examines the $\hat{G}$ operator in the limit of $\tau_c \gg T_{oc}$ then $\hat{G} \to \hat{T}$ and Eq. (1) is recovered. More importantly, in the same limit Eq. (14) reduces to the result derived in Ref. [27], which uses an operator expansion in time that requires the condition $\omega_0\tau_c \gg 1$ to converge. Note that such a condition would not be satisfied for the lower collision times listed in Table I. Additionally, in the extreme limit of zero dissipation (i.e., $\tau_c \to \infty$), then $j_{fc}(\vec{x},t) \to i(q/m\omega_0)\hat{T}^{-1}[\rho(\vec{x},t)\xi(\vec{x},t)]$, which is the limiting case for a plasma of noninteracting particles [38].

D. The modified NLSE

To fully characterize Eq. (10), a form for the nonlinear polarization envelope must be specified. In this work the nonlinear polarization derived in Ref. [20] is selected. Combining this with the free-carrier and photoionization currents derived in Secs. II B and II C a modified NLSE is obtained,

$$\frac{\partial\xi}{\partial z'} = \frac{i}{2k_0}\hat{T}^{-1}\nabla_\perp^2\xi + i\hat{D}_b\xi + i\frac{k_0\epsilon_0 c n_2}{2}(1-f_r)\hat{T}|\xi|^2\xi + i\frac{k_0\epsilon_0 c n_2}{2}f_r\hat{T}\left[\int_{-\infty}^{\tau} d\tau' R(\tau-\tau')|\xi(\tau')|^2\right]\xi - \frac{\sigma}{2}(1+i\omega_0\tau_c)\hat{G}^{-1}[\rho\xi] - \frac{W_{\mathrm{PI}}U}{2I}\xi. \quad (16)$$

Here, n_2 is the intensity-based nonlinear index of refraction, f_r is the fraction of the Raman contribution to the nonlinear polarization, and $R(\tau)$ is the Raman response function derived in Ref. [20],

$$R(\tau) = \frac{\tau_1^2+\tau_2^2}{\tau_1\tau_2^2}\, e^{-\tau/\tau_2}\, \sin(\tau/\tau_1),$$

where the constants τ_1 and τ_2 are adjustable parameters chosen to provide an adequate fit with the Raman-gain spectrum [16]. The nonlinear polarization term in Eq. (16) now accounts for self-focusing, self-steepening (nonlinear shock), and stimulated Raman scattering. It should be emphasized that some recent works suggest that saturation of nonlinear refractive effects may occur via fifth-order processes at intensities approaching 10^{18} W/cm^2, particularly in air [39,40]. In such cases higher-order effects should be included in the nonlinear polarization envelope. However, this article will henceforth give special consideration only to materials where the nonlinear polarization of Ref. [20] has demonstrated good agreement with experiment. For such materials, Eq. (16) is the modified NLSE we propose as the generally correct choice for ultrashort pulse propagation through regions of dense plasma. The remainder of this article will explore the significant differences that arise from using Eq. (1) as the free-carrier contribution to the modified NLSE instead of Eq. (2) and how such differences might arise in experiment.

III. ANALYSIS OF FREE-CARRIER CONTRIBUTIONS TO THE MODIFIED NLSE

This section will explore the predictions of Eqs. (1) and (2) as descriptions of free-carrier optical effects. It is instructive to examine the corrections to absorption and phase separately when time derivatives of the complex field envelope are present. Therefore, by taking the free-carrier temporal correction operators $\hat{T}^{-1}$ and $\hat{G}^{-1}$ to first order, the changes in intensity, I, and spatio-temporal phase, ϕ, with respect to the propagation axis are:

$$\left[\frac{\partial I}{\partial z'}\right]_{fc} = -\sigma\rho I - \sigma\beta\tau_c\left[\dot{\rho}I + \rho\frac{\dot{I}}{2}\right] - \sigma\rho I\eta\frac{\dot{\phi}}{\omega_0} \quad (17a)$$

$$\left[\frac{\partial \phi}{\partial z'}\right]_{fc} = -\frac{\sigma}{2}\omega_0\tau_c\rho + \frac{\sigma\eta}{2\omega_0}\left[\frac{\rho\dot{I}}{2I} + \dot{\rho}\right] - \frac{\sigma}{2}\beta\tau_c\rho\dot{\phi}, \quad (17b)$$

where all dotted terms indicate time derivatives, and β and η are dimensionless constants that again distinguish between the descriptions of Eqs. (1) and (2). Table II lists the values for the constants η and β for three different descriptions of free-carrier effects. If Eq. (1) is chosen as a description of free-carrier effects then these constants are simply $\beta = \eta = 1$ and this description will henceforth be referred to as model I. If instead Eq. (2) is chosen as a description of free-carrier effects then the two constants are related by $\eta = \beta + 1$ where $\beta = (\omega_0^2\tau_c^2 - 1)/(1 + \omega_0^2\tau_c^2)$ and this will be referred to as model II. Additionally, a zeroth temporal order approximation of both models I and II ($\hat{T}^{-1} = 1$ and $\hat{G}^{-1} = 1$, respectively) is shown for comparison and will be referred to as model III. In this case there are no time derivative corrections to the free-carrier contribution and the constants are therefore $\eta = \beta = 0$. Table II also introduces a color scheme (online) that will be used to distinguish between the three models in the data to be presented throughout this article: model I shown in blue, model II shown in red, and model III shown in black.

Figure 2 shows the numerical value of β as a function of τ_c/T_{oc} for model II. As expected, for collision times of one optical cycle or less, the value of β for model II shows considerable deviation from unity, and thus models I and II are not in agreement in this regime. For collision times greater than two optical cycles, Fig. 2 shows that models I and II will be in very good agreement on the value of $\beta = 1$. However, agreement between the models for the constant η is a very different matter. In fact, models I and II only agree on the value of η at a single collision time of $\tau_c = \omega_0^{-1}$, which is only a fraction of an optical cycle and simultaneously where $\beta = 0$ for model II. Furthermore, models I and II will disagree on the value of η by a factor of two for any collision

TABLE II. Three different models of free-carrier effects used in this article and their respective values for the constants η and β in Eq. (17).

Model I (red online)	Model II (blue online)	Model III (black online)
Eq. (1)	Eq. (2)	Eq. (1), $\hat{T}^{-1} = 1$
$\eta = 1$	$\eta = \beta + 1$	$\eta = 0$
$\beta = 1$	$\beta = (\omega_0^2\tau_c^2 - 1)/(1 + \omega_0^2\tau_c^2)$	$\beta = 0$

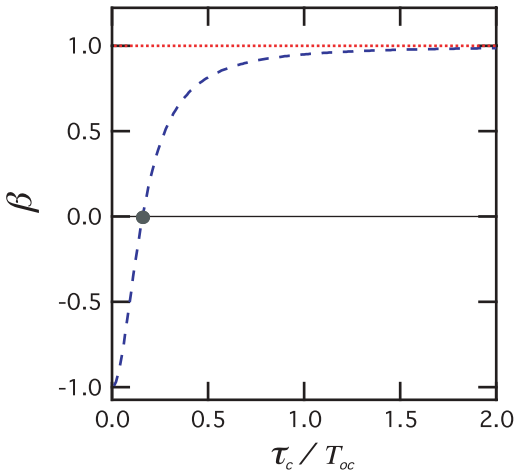

FIG. 2. (Color online) The dimensionless constant β for model II as a function of the collision time scaled by the optical cycle of the applied field. The dotted red line represents model I, the dashed blue line represents model II, and the solid black line represents model III, shown for comparison. The grey dot indicates the collision time at which models II and III are in exact agreement for the value of $\beta = 0$.

time greater than two optical cycles, thereby extending the range of collision times where such differences could be significant. Here it is important to recall that the cross section of inverse Bremsstrahlung absorption, σ, is also a function of the collision time and will decay as the imaginary part of g decays for increasing τ_c (see dashed line in Fig. 1). This ensures that differences between the respective calculations of η will become gradually less significant as one approaches the limit of small dissipation (i.e., $\tau_c \gg T_{oc}$).

Equation (17) allows one to determine which pulse attributes will accentuate the differences between models I and II. For example, a strongly chirped pulse ($\dot{\phi} \sim \pm\omega_0$) will make contributions to the spatio-temporal phase [the third term on the right-hand side of Eq. (17b)] equal in magnitude to that of the zeroth temporal order [first term on the right-hand side of Eq. (17b)]. However, in the case where $\tau_c = \omega_0^{-1}$ this entire contribution is eliminated in model II because $\beta = 0$ under that description. The same is true for the plasma generation and pulse steepening term of Eq. (17a), the second term on the right-hand side. If instead collision times greater than one optical cycle are adopted, then $\beta \approx 1$ for models I and II while their respective values for the constant η differ by a factor of two. Here, strongly chirped pulses will make contributions to plasma absorption [Eq. (17a)] of similar magnitude to the zeroth temporal order, but the chirp contribution of model II will be twice as strong as the model I contribution. Analogously, the same is true for the plasma generation and pulse steepening terms of Eq. (17b).

It should be emphasized that any dissimilarities between the models of free-carrier effects will be comparatively stronger on the trailing edge of the pulse, because the plasma density ρ has had more time to accumulate. Note that on the trailing edge of the pulse, $\dot{I}$ will be negative by definition, while the sign of the plasma generation rate $\dot{\rho}$ will depend on the description one uses to calculate ρ as a function of time. Also, it will often be the case that $\dot{\phi}$ will be negative on the trailing edge of the pulse due to self-phase modulation ($\dot{\phi} \sim n_2\dot{I}$) and

plasma-induced blue shifting [23,41]. Under such conditions, Eq. (17) predicts that model I will significantly mischaracterize the effects of plasma absorption and defocusing on the trailing edge of the pulse. It is notable that the value of the collision time has been interpreted as a measure to characterize the balance between plasma absorption and plasma defocusing [7]. This being the case, model I will significantly mischaracterize the balance of plasma absorption and defocusing for a large range of collision times currently used in the literature. These effects are detectable by examining phase accumulation and energy absorption during ultrashort pulse propagation, which is addressed using numerical simulation as described in the next section.

IV. DESCRIPTION OF SIMULATIONS

In order to explore how the different models of free-carrier effects compare with other ultrashort optical processes, simulations have been performed solving Eq. (16) in fused silica at a peak laser wavelength of 800 nm. This material and wavelength were chosen because the optical properties of fused silica are well characterized in the literature for 800-nm light. Additionally, Table I shows that the values of the collision time for fused silica used in the literature span over three orders of magnitude, encompassing collision times much less than, on the order of, and much greater than a single optical cycle for an 800-nm field, making it an ideal material for this study. Table III lists the optical and material parameters that are used for every simulation reported in this article.

Discrepancies between models I and II are examined by simulating the propagation of ultrashort pulses through 100 μm of fused silica. These simulations have been organized to search for such differences over a variety of pulsewidths and collision times. Differences in the results predicted by models I and II should scale inversely with the pulsewidth. Therefore, simulations are performed for pulses with full width half-maximum (FWHM) pulsewidths of $\tau_{\text{fwhm}} = 10$, 20, and 40 fs. For each value of the pulsewidth, simulations are performed at 15 free-carrier collision times ranging from 0.2–16.0 fs (i.e., 0.075–6 optical cycles), thus encompassing most of the collision times found in Table I. Finally, for each pulsewidth and collision time category, three simulations are performed using models I, II, and III, respectively, to describe free-carrier effects, making a total of 135 simulations. The initial energy for each pulse was appropriately selected to obtain an incident peak intensity of 5.3×10^{13} Wcm^{-2}. Under the assumption of a flat spatio-temporal phase and cylindrical beam symmetry our initial electric field envelope is then assigned the form,

$$\xi(r, \tau, z = 0) = \xi_0 \exp\left(-\frac{r^2}{w_r^2} - \frac{2\ln(2)\tau^2}{\tau_{\text{fwhm}}^2}\right), \tag{18}$$

where $\xi_0 = \sqrt{2I_0/n_0\epsilon_0 c}$.

In solving Eq. (16) it is necessary to simultaneously solve a rate equation for the free-carrier plasma density ρ as a function of space and time [42],

$$\frac{\partial \rho}{\partial t} = W_{\text{PI}}(|\xi|). \tag{19}$$

In this article photoionization is considered as the only generator of free carriers, noting a recent work that found avalanching (impact ionization) to be negligible in fused silica for pulses as short as 90 fs at the intensities under consideration [25]. In principle, however, impact ionization can also be added. Additionally, our generated free-electron densities are at least two orders of magnitude below the molecular density of fused silica, 2.2×10^{22} cm^{-3} [5]. Therefore, a full valance band is assumed throughout.

The choice of a model for the photoionization rate should be made with great care. In this work, we choose the photoionization rate for solids developed by Keldysh [43] because in numerous studies it has provided good agreement with experiments of ultrashort laser pulse propagation in fused silica [5,7,24,25,29,44–48]. The photoionization formula $W_{\text{PI}}(|\xi|)$ developed by Keldysh is [43]

$$W_{\text{PI}}(|\xi|) = \frac{2\omega_0}{9\pi}\left(\frac{m\omega_0}{\sqrt{\gamma_1}\,\hbar}\right)^{3/2} Q(\gamma, x)\exp\left(-\varpi\langle x+1\rangle\right). \tag{20}$$

Here, the Keldysh parameter $\gamma = \omega_0\sqrt{mU/e_0|\xi|}$, $\gamma_1 = \gamma^2/(1+\gamma^2)$, $\gamma_2 = 1-\gamma_1$, $\varpi = \pi(K(\gamma_1) - E(\gamma_2))/E(\gamma_2)$, and $x = (2U/\pi\omega_0)(\sqrt{1-\gamma^2}/\gamma)E(\gamma_2)$. The notation $\langle\cdot\rangle$ denotes the integer part, and the functions $K(x)$ and $E(x)$ are complete elliptical integrals of the first and second kind, respectively, as defined in Ref. [49]. The function $Q(\gamma, x)$ is given by

$$Q(\gamma, x) = \sqrt{\frac{\pi}{2K(\gamma_2)}}\sum_{n=0}^{\infty}\exp\left(-n\varpi\right)\Phi\left(\sqrt{\vartheta(n+2\nu)}\right),$$

where $\vartheta = \pi^2/4K(\gamma_2)E(\gamma_2)$, $\nu = \langle x+1\rangle - x$, and $\Phi(z) = \int_0^z \exp(y^2 - z^2)dy$ is the Dawson function.

The solid line in Fig. 3 shows the Keldysh photoionization rate as a function of the optical intensity in fused silica for parameters listed in Table III. Note that the Keldysh parameter γ is used to distinguish between the domains of multiphoton ionization (MPI), $\gamma \gg 1$, and tunneling ionization, $\gamma \ll 1$. In our simulations, the condition $\gamma = 1$ is satisfied at an intensity of 2.7×10^{13} W/cm^2. The dashed line in Fig. 3

TABLE III. A list of the optical and material parameters used for all the simulations reported in this article. Material parameters are those for fused silica [5].

Symbol	Description	Value	Units
λ	Initial wavelength	800	nm
w_r	Initial beam waist	75	μm
I_0	Initial peak intensity	5.3×10^{13}	Wcm^{-2}
L_z	Sample length	100	μm
n_0	Linear refractive index	1.45	
k_2	GVD coefficient	361	fs^2 cm^{-1}
n_2	Nonlinear refractive index	2.48×10^{-16}	cm^2 W^{-1}
f_r	Raman response fraction	0.18	
τ_1	Raman sinusoidal time	12.2	fs
τ_2	Raman decay time	32	fs
U	Material band gap	9	eV
m	Reduced electron-hole mass	0.5	m_e
e_0	Free-carrier charge	1.602×10^{-19}	C

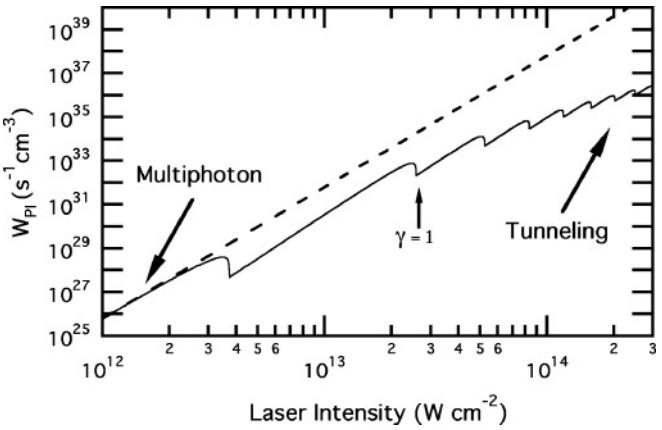

FIG. 3. Photoionization rate as a function of optical intensity in fused silica according to the theory of Keldysh. The solid line shows the full Keldysh expression, while the dashed line shows the common multiphoton ionization approximation valid at low intensities. Optical and material parameters used to calculate this rate are those from Table III.

shows the Keldysh MPI rate: $W_{\rm PI} = \sigma_6 I^6$, where $\sigma_6 = 6.04 \times 10^{-47}({\rm cm}^2/{\rm W})^6\,{\rm s}^{-1}{\rm cm}^{-3}$ for our chosen parameters. Because our simulations never exceed their initial peak intensity of $5.3 \times 10^{13}\,{\rm W/cm}^2$, most of our pulses lay in the domain of multiphoton ionization. However, our peak intensities are too high to be accurately modeled by the MPI rate and yet too weak to be in the tunneling regime. Therefore, the full Keldysh photoionization formula is used throughout.

For our simulations it was sufficient to set the bound charge dispersion operator $\hat{D}_b = -i(k_2/2)\partial_\tau^2$, as no linear absorption from bound charges is assumed ($\alpha_m = 0$), and higher linear dispersion terms were found to have no significant effect when included. In fact, even group velocity dispersion had only small effects, because the propagation distance of 100 μm is very small compared to the group velocity dispersion (GVD) length $L_{\rm GVD} = \tau_{\rm fwhm}^2/|k_2| \sim 1$ cm for our shortest pulse. Additionally, a relatively large beam waist of 75 μm was chosen for a peak intensity of $5.3 \times 10^{13}\,{\rm Wcm}^{-2}$. This was done in an effort to reduce the influence of spatial diffraction and allow us to concentrate on how ultrashort free-carrier effects compare with other nonlinear optical processes. Equation (16) is solved using a split step method, with the first two terms of the right-hand side constituting a "linear" step and the rest of the terms constituting a "nonlinear" step. Equation (16) is solved simultaneously with Eq. (19) which is in turn solved using a fourth-order Runge-Kutta method.

V. RESULTS

Figure 4 shows the total transmittivity as a function of the free-carrier collision time after propagating through a $100 - \mu$m sample of fused silica. For $\lambda = 800$ nm, one optical cycle is ≈ 2.67 fs; the values of τ_c in Fig. 4 range from 0.075 to 6 optical cycles (0.2–16 fs), covering three orders of magnitude in order to sample the wide range of collision times listed for fused silica in Table I. The transmittivity plots are shown for each of the three initial pulses with FWHM pulsewidths of 10, 20, and 40 fs. Each plot in the figure shows results from the free-carrier descriptions of model I (dotted line),

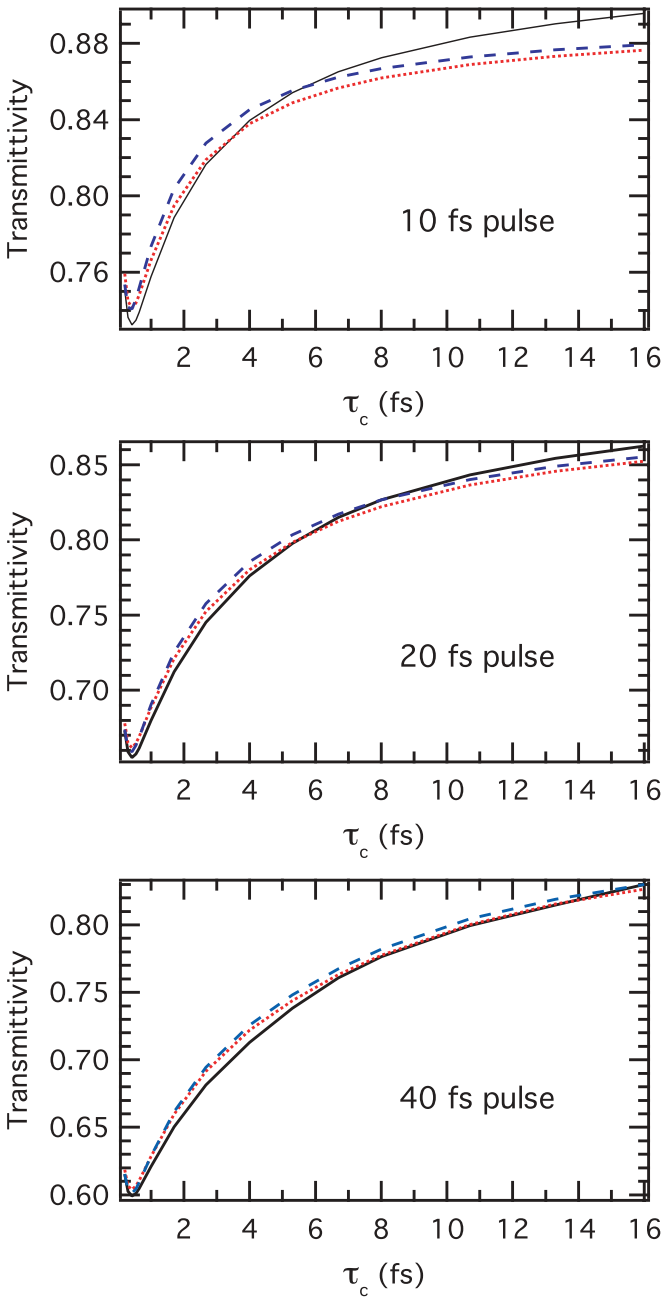

FIG. 4. (Color online) Total transmittivity after propagating through 100 μm of fused silica shown for 10-, 20-, and 40-fs pulses. Transmittivity is shown as a function of the free-carrier collision time. The dotted red line represents model I, the dashed blue line represents model II, and the solid black line represents model III shown for comparison.

model II (dashed line), and model III (the zeroth temporal order approximation of models I and II, shown for comparison as a solid line). These are further distinguished by an online color scheme of red, blue, and black, respectively (i.e., the convention introduced in Table II). Note the discrepancies in transmittivity on the order of 1% that occur between models I and II for a 10-fs pulse. Equally notable is the fact that this difference in transmittivity can be seen over the large range of collision times ranging from approximately 1 fs and finally

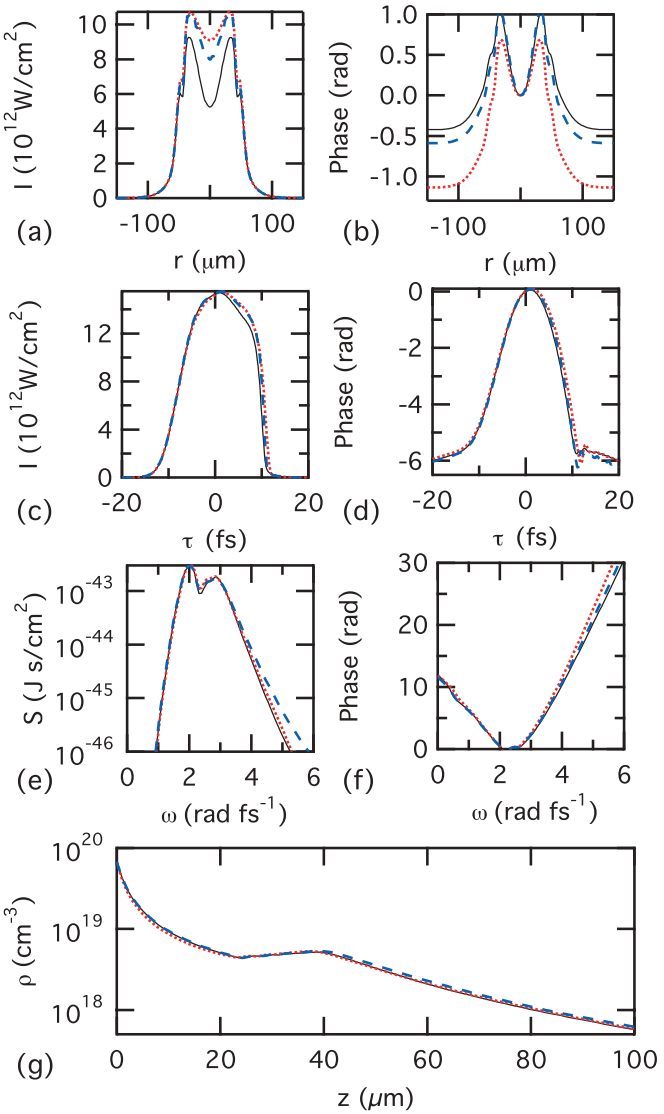

FIG. 5. (Color online) Selected results of a 10-fs pulse after propagating through 100 μm of fused silica with a free-carrier collision time of 0.42 fs. The dotted red line represents model I, the dashed blue line represents model II, and the solid black line represents model III. (a) and (b) show the spatial intensity and phase at the trailing edge of the pulse ($\tau = 10$ fs), (c) and (d) show the temporal intensity and phase at the spatial center ($r = 0$), (e) and (f) show the spectral intensity and phase at the spatial center ($r = 0$), and (g) shows the peak plasma density as a function of the propagation distance.

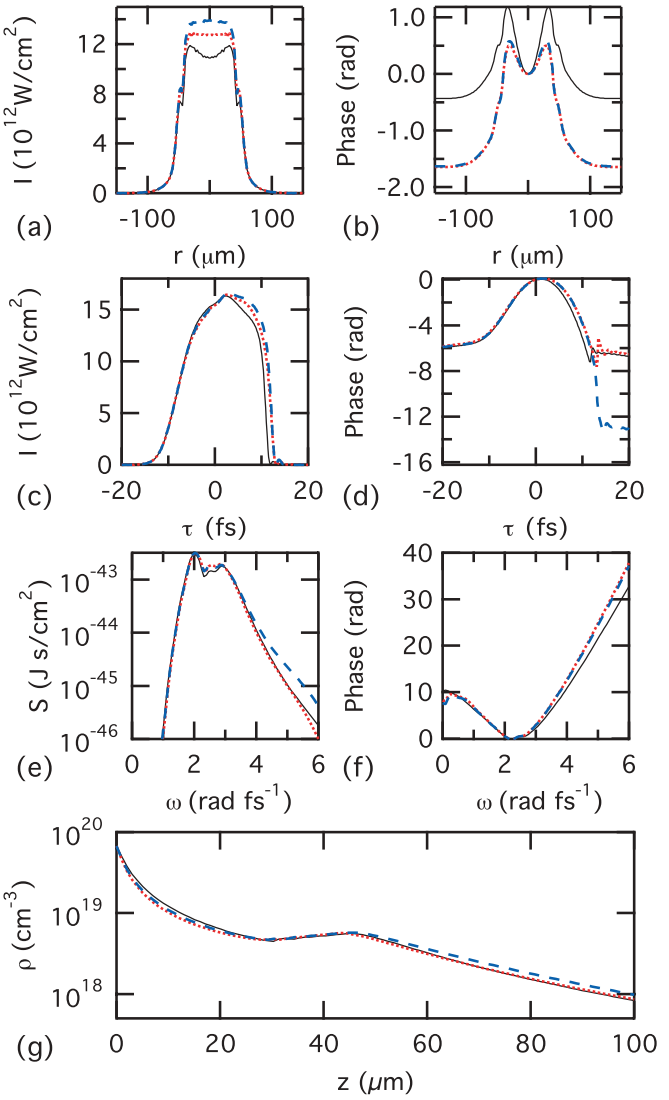

FIG. 6. (Color online) Selected results of a 10-fs pulse after propagating through 100 μm of fused silica with a free-carrier collision time of 1.0 fs. The dotted red line represents model I, the dashed blue line represents model II, and the solid black line represents model III. (a) and (b) show the spatial intensity and phase at the trailing edge of the pulse ($\tau = 10$ fs), (c) and (d) show the temporal intensity and phase at the spatial center ($r = 0$), (e) and (f) show the spectral intensity and phase at the spatial center ($r = 0$), and (g) shows the peak plasma density as a function of the propagation distance.

converging at about 16 fs. This range of discrepancy extends over 5.5 optical cycles of collision time and is the direct result of the pulse chirp term in Eq. (17a), which demonstrates that only instantaneous frequency shifts can cause discrepancies of this kind for collision times greater than one optical cycle. These differences also occur for the 20- and 40-fs pulse transmittivity plots. As expected, pulses with the same initial intensity but a longer pulsewidth will ultimately decrease the magnitude of all field time derivative corrections.

To show specific discrepancies arising in intensity and phase at the trailing edges of the pulses, results from some of the most instructive simulations are examined. Figures 5–8 show selected intensity and phase profiles, comparing the three aforementioned models of free-carrier effects using the same graphing and online color convention introduced in Table II. These figures are organized in an identical manner to display the spatial intensity at the trailing edge of the pulse, $I(r, \tau = +\tau_{\mathrm{fwhm}})$; the temporal intensity at the spatial center, $I(r = 0, \tau)$; the spectral intensity at the spatial center, $S(r = 0, \omega) = (1/2)n_0\epsilon_0 c|\tilde{\xi}(r = 0, \omega - \omega_0)|^2$; and the corresponding phase for each intensity. Also shown is the maximum plasma density as a function of the propagation distance. Note that all maximum plasma densities are at least an order of magnitude below the threshold of permanent

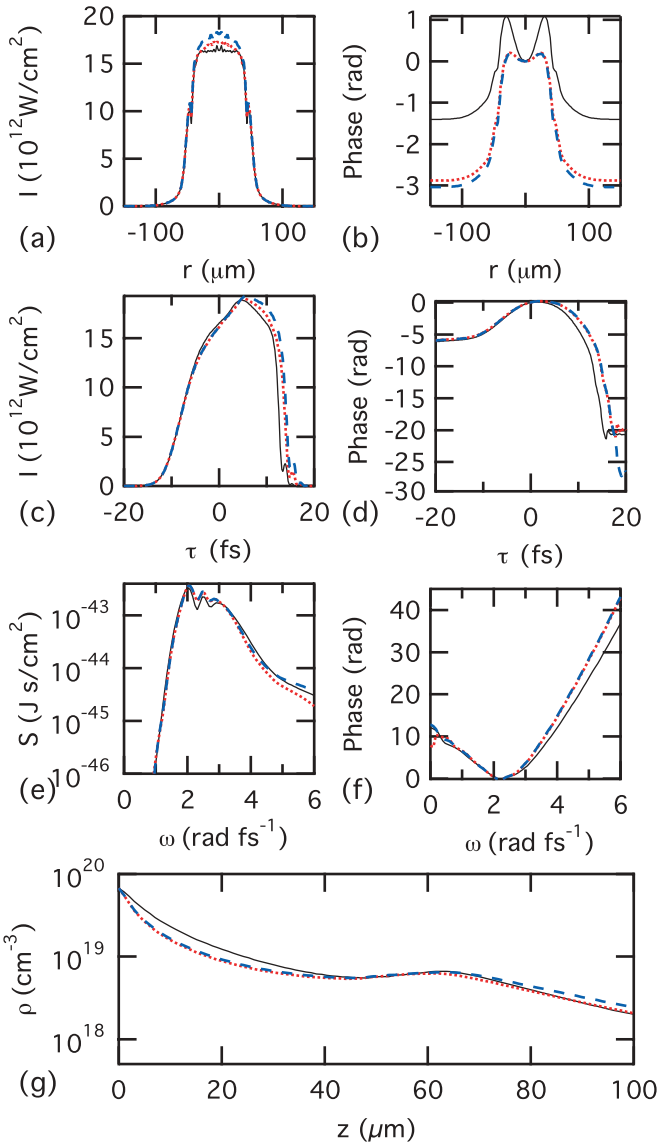

FIG. 7. (Color online) Selected results of a 10-fs pulse after propagating through 100 μm of fused silica with a free-carrier collision time of 2.6 fs. The dotted red line represents model I, the dashed blue line represents model II, and the solid black line represents model III. (a) and (b) show the spatial intensity and phase at the trailing edge of the pulse ($\tau = 10$ fs), (c) and (d) show the temporal intensity and phase at the spatial center ($r = 0$), (e) and (f) show the spectral intensity and phase at the spatial center ($r = 0$), and (g) shows the peak plasma density as a function of the propagation distance.

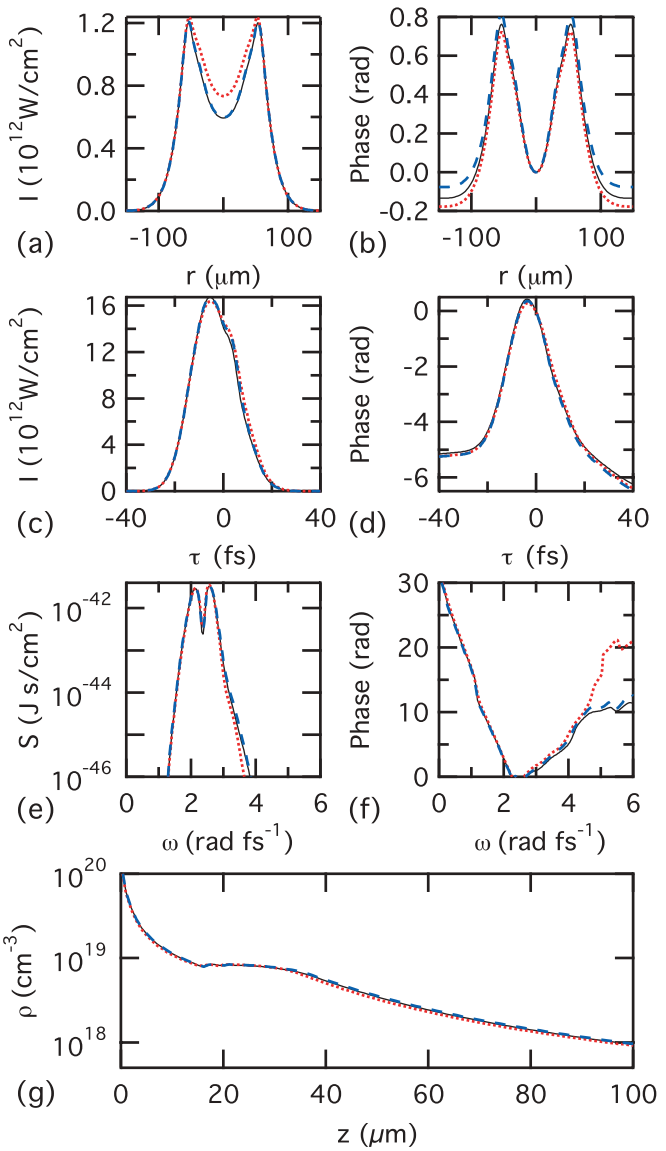

FIG. 8. (Color online) Selected results of a 20-fs pulse after 100 μm of propagation in fused silica with a free-carrier collision time of 0.42 fs. The dotted red line represents model I, the dashed blue line represents model II, and the solid black line represents model III. (a) and (b) show the spatial intensity and phase at the trailing edge of the pulse ($\tau = 20$ fs), (c) and (d) show the temporal intensity and phase at the spatial center ($r = 0$), (e) and (f) show the spectral intensity and phase at the spatial center ($r = 0$), and (g) shows the peak plasma density as a function of the propagation distance.

structural damage in fused silica, and yet frequently above a recently established value for reversible refractive index modification [7].

Figure 5 shows results from 10-fs pulse propagation for a collision time of 0.42 fs. The collision time of 0.42 fs ($\tau_c = \omega_0^{-1}$) is of special significance, as the constant β in Eq. (17) equals zero for model II. As discussed in Sec. III, this collision time results in a significant disagreement between the two free-carrier dispersion descriptions on the contribution from plasma generation and pulse steepening to energy absorption, as well as the contribution of instantaneous frequency shift (pulse chirp) to the spatio-temporal phase at this collision time. Plots (a) and (b) of Fig. 5(f) show how strong this disagreement becomes at the trailing edge of the pulse where the plasma density is highest. Although the differences in the spatial intensity are indeed noticeable, it is the spatial phase that displays the largest discrepancy between the descriptions of free-carrier effects in Fig. 5. It is evident from the temporal phase in Fig. 5(d) (due largely to self-phase modulation) that there is an average temporal chirp of $\dot{\phi} \approx -\omega_0/4$ on the trailing edge of the pulse. The last term in Eq. (17b) explains how the presence of such a strong temporal chirp at the trailing edge

of the pulse leads to better agreement between models II and III than with model I in spatial phase, because $\beta = 0$ for both models II and III, whereas $\beta = 1$ for model I.

Figures 6 and 7 show results from 10-fs pulse propagation in a material with electron collision times of 1.0 and 2.67 fs, respectively. For both of these collision times, Figs. 6(b) and 7(b) show little or no difference between the free-carrier models in the spatial phase at the trailing edge of the pulse. However, these figures do reveal very subtle differences between the free-carrier descriptions in the plots of temporal intensity, temporal phase, and spectra and maximum plasma densities.

Figure 8 shows selected profiles for 20-fs pulse propagation with collision times of 0.42 fs. Comparison of Figs. 5(b) and 8(b) demonstrates how doubling the pulsewidth dramatically reduces the discrepancies between the three free-carrier descriptions. Although a small difference in spatial intensity is retained in Fig. 8(a), all other intensity and phase profiles, as well as the maximum plasma densities, of models I and II are in very good agreement with the zeroth temporal order approximation description of model III. This makes the discrepancies between the free-carrier descriptions at higher pulsewidths and collision times in Fig. 4 most interesting because such differences, though difficult to detect in an individual profile will, upon integration over the entire pulse intensity, yield noticeable changes in the total pulse energy. At longer pulsewidths or higher intensities, plasma densities sufficient to cause permanent optical damage will occur, increasing the magnitude of these discrepancies. A study of such effects, however, would likely necessitate the inclusion of avalanching in the temporal evolution of the free-carrier plasma. The process of impact ionization depends sensitively on the description of free-carrier absorption [12,50,51], which in turn can be significantly influenced by ultrashort effects, as demonstrated by Eq. (17a). The significance of temporal corrections to the avalanching contribution have yet to be addressed in the literature to our knowledge. Such an investigation is currently planned as a future study.

VI. CONCLUSION

A modified nonlinear Schrödinger equation has been derived that includes a free-carrier contribution calculated from the Drude model. Intrinsic to this calculation is an inverse free-charge dispersion operator whose expansion converges for all values of the free-carrier collision time, as well as for laser pulses as short as a single optical cycle in duration. It therefore retains all of the specified information about free-charge dispersion contributions without resorting to a limiting case, and will provide an accurate description of a Drude free-carrier current density wherever the modified NLSE is valid. Our derived free-carrier current density and the dispersion relations contained therein are shown to converge to the other descriptions of ultrashort free-carrier current densities currently in use in the literature for the limiting case in which the collision time is much greater than an optical cycle. If, however, the free-carrier collision time is on the order of one optical cycle or less, then significant differences in plasma absorption and defocusing may arise for pulses that are strongly chirped or steepened.

Collision times in the range of one optical cycle or less are frequently cited or measured in the literature, while the use of ultrashort pulses with steep edges and large frequency shifts are ubiquitous. Our simulations suggest that strongly chirped ultrashort pulses, with an instantaneous frequency shift comparable to the carrier frequency, may effect changes to energy absorption and phase accumulation that only the free-carrier dispersion relations derived in this article are adequate to explain. As the study of laser-induced damage and laser-plasma interactions further engages the use of ultrashort pulses that approach the domain of a single optical cycle, this work should provide a more general and complete method for describing free-carrier dispersion relations in the context of a nonlinear envelope propagation equation.

ACKNOWLEDGMENTS

The authors thank Tom Lanier and Sebastian Winkler for many useful discussions.

[1] A. Vogel, J. Noack, G. Huttman, and G. Paltauf, Appl. Phys. B **81**, 1015 (2005).
[2] Y. Shimotsuma, P. G. Kazansky, J. Qiu, and K. Hirao, Phys. Rev. Lett. **91**, 247405 (2003).
[3] C. B. Schaffer, A. Brodeur, J. F. Garcia, and E. Mazur, Opt. Lett. **26**, 93 (2001).
[4] C. B. Schaffer and E. Mazur, Opt. Photonics News **12**, 20 (2001).
[5] S. W. Winkler, I. M. Burakov, R. Stoian, N. M. Bulgakova, A. Husakou, A. Mermillod-Blondin, A. Rosenfeld, D. Ashkenasi, and I. V. Hertel, Appl. Phys. A **84**, 413 (2006).
[6] X. Zhu, A. Y. Naumov, D. M. Villeneuve, and P. B. Corkum, Appl. Phys. A **69**, S367 (1999).
[7] A. Couairon, L. Sudrie, M. Franco, B. Prade, and A. Mysyrowicz, Phys. Rev. B **71**, 125435 (2005).
[8] T. Brabec and F. Krausz, Rev. Mod. Phys. **72**, 545 (2000), http://www.springerlink.com/content/yudy1xel4d317vae.
[9] T. Brabec and F. Krausz, Phys. Rev. Lett. **78**, 3282 (1997).
[10] T. Q. Jia, H. Y. Sun, X. X. Li, D. H. Feng, C. B. Li, S. Z. Xu, R. X. Li, Z. Z. Xu, and H. Kuroda, J. Appl. Phys. **100**, 023103 (2006).
[11] A. Rosenfeld, M. Lorenz, R. Stoian, and D. Ashkenasi, Appl. Phys. A **69**, S373 (1999).
[12] B. Rethfeld, Phys. Rev. Lett. **92**, 187401 (2004).
[13] C. B. Schaffer, A. Brodeur, and E. Mazur, Meas. Sci. Technol. **12**, 1784 (2001).
[14] R. W. Boyd, *Nonlinear Optics* (Academic, London, 1992).
[15] J. Satsuma and N. Yajima, Prog. Theor. Phys. Suppl. **55**, 284 (1974).
[16] J. H. Marburger, Prog. Quantum Electron. **4**, 35 (1975).
[17] Y. R. Shen, *The Principles of Nonlinear Optics* (John Wiley and Sons, New York, 1984).
[18] G. P. Agrawal, *Nonlinear Fiber Optics*, 2nd ed. (Academic Press, San Diego, 1995).
[19] R. L. Sutherland, *Handbook of Nonlinear Optics*, 2nd ed. (Dekker, New York, 2003).
[20] K. J. Blow and D. Wood, J. Quantum Electron. **25**, 2665 (1989).

[21] A. Couairon, E. Gaizauskas, D. Faccio, A. Dubietis, and P. D. Trapani, Phys. Rev. E **73**, 016608 (2006).
[22] S. Tzortzakis, L. Sudrie, M. Franco, B. Prade, A. Mysyrowicz, A. Couairon, and L. Bergé, Phys. Rev. Lett. **87**, 213902 (2001).
[23] A. Couairon, G. Mechain, S. Tzortzakis, M. Franco, B. Lamouroux, B. Prade, and A. Mysyrowicz, Opt. Commun. **225**, 177 (2003).
[24] L. Sudrie, A. Couairon, M. Franco, B. Lamouroux, B. Prade, S. Tzortzakis, and A. Mysyrowicz, Phys. Rev. Lett. **89**, 186601 (2002).
[25] A. Q. Wu, I. H. Chowdhury, and X. Xu, Phys. Rev. B **72**, 085128 (2005).
[26] S. Skupin, G. Stibenz, L. Berge, F. Lederer, T. Sokollik, M. Schnurer, N. Zhavoronkov, and G. Steinmeyer, Phys. Rev. E **74**, 056604 (2006).
[27] S. Skupin and L. Berge, Physica D **220**, 14 (2006).
[28] A. Couairon, S. Tzortzakis, L. Bergé, M. Franco, B. Prade, and A. Mysyrowicz, J. Opt. Soc. Am. B **19**, 1117 (2002).
[29] P. Polesana, A. Dubietis, M. A. Porras, E. Kucinskas, D. Faccio, A. Couairon, and P. D. Trapani, Phys. Rev. E **73**, 056612 (2006).
[30] S. Akturk, C. D'Amico, M. Franco, A. Couairon, and A. Mysyrowicz, Phys. Rev. A **76**, 063819 (2007).
[31] P. Polesana, M. Franco, A. Couairon, D. Faccio, and P. D. Trapani, Phys. Rev. A **77**, 043814 (2008).
[32] A. L. Gaeta, Phys. Rev. Lett. **84**, 3582 (2000).
[33] J. D. Jackson, *Classical Electrodynamics*, 3rd ed. (John Wiley & Sons, Chichester, NY, 1998).
[34] J. R. Gulley, S. W. Winkler, and W. M. Dennis, Opt. Eng. **47**, 054302 (2008).
[35] X. Mao, S. S. Mao, and R. E. Russo, Appl. Phys. Lett. **82**, 697 (2003).
[36] D. Giguère, G. Olivié, F. Vidal, S. Toetsch, G. Girard, T. Ozaki, J.-C. Kieffer, O. Nada, and I. Brunette, J. Opt. Soc. Am. A **24**, 1562 (2007).
[37] Q. Sun, H. Jiang, Y. Liu, Z. Wu, H. Yang, and Q. Gong, Opt. Lett. **30**, 320 (2005).
[38] C. Courtois, A. Couairon, B. Cros, J. R. Marques, and G. Matthieussent, Phys. Plasmas **8**, 3445 (2001).
[39] V. Loriot, E. Hertz, O. Faucher, and B. Lavorel, Opt. Express **17**, 13429 (2009).
[40] M. Nurhuda, A. Suda, and K. Midorikawa, New J. Phys. **10**, 053006 (2008).
[41] S. S. Mao, F. Quéré, S. Guizard, X. Mao, R. E. Russo, G. Petite, and P. Martin, Appl. Phys. A: Mater. Sci. Process. **79**, 1695 (2004).
[42] B. C. Stuart, M. D. Feit, S. Herman, A. M. Rubenchik, B. W. Shore, and M. D. Perry, Phys. Rev. B **53**, 1749 (1996).
[43] L. V. Keldysh, Sov. Phys. JETP **20**, 1307 (1965) [Zh. Eksp. Teor. Fiz. **47**, 1945 (1964)].
[44] L. Berge, S. Skupin, and G. Steinmeyer, Phys. Rev. Lett. **101**, 213901 (2008).
[45] B. H. Christensen and P. Balling, Phys. Rev. B **79**, 155424 (2009).
[46] A. Kaiser, B. Rethfeld, M. Vicanek, and G. Simon, Phys. Rev. B **61**, 11437 (2000).
[47] J. Liu, R. Li, and Z. Xu, Phys. Rev. A **74**, 043801 (2006).
[48] M. Mero, J. Liu, W. Rudolph, D. Ristau, and K. Starke, Phys. Rev. B **71**, 115109 (2005).
[49] M. Abramowitz and I. A. Stegun, *Handbook of Mathematical Functions*, 10th ed. (Dover, New York, 1972).
[50] B. Rethfeld, Phys. Rev. B **73**, 035101 (2006).
[51] L. Jiang and H.-L. Tsai, J. Heat Transfer **128**, 926 (2006).